Polymer Chemistry

PAPER

View Article Online
View Journal | View Issue

Cite this: *Polym. Chem.*, 2015, **6**, 6227

A cross-linkable triphenylamine derivative as a hole injection/transporting material in organic light-emitting diodes†

Hsi-Kang Shih,[a] Yu-Lin Chu,[a] Feng-Chih Chang,[a,b] Chao-Yuan Zhu*[a] and Shiao-Wei Kuo*[b]

We have synthesized TPABZ, a new thermally cross-linkable triphenylamine derivative containing a benzoxazine functional group, for application in organic light-emitting diodes (OLEDs). We used differential scanning calorimetry, thermogravimetric analysis, UV–Vis spectroscopy, and cyclic voltammetry to investigate the thermal, physical, and electrochemical properties of TPABZ, which is readily polymerized, through ring-opening polymerization of its benzoxazine unit, upon heating at 220 °C for 30 min. The cured TPABZ (P-TPABZ) is suitable for use as a hole injection/transport material in OLEDs because it has an appropriate HOMO energy level (–5.16 eV) to form a stepwise energy ladder and a high LUMO energy level (–1.68 eV) with great potential for electron blocking. We fabricated multilayered OLEDs (ITO/TPABZ or P-TPABZ/NPB/Alq_3/LiF/Al) through successive spin-coating and vacuum deposition processes; the device incorporating P-TPABZ exhibited good performance (EQE: 2.44%; LE_{max}: 8.42 cd A^{-1}; PE_{max}: 4.34 lm W^{-1}).

Received 9th June 2015,
Accepted 16th July 2015

DOI: 10.1039/c5py00882d

www.rsc.org/polymers

Introduction

Organic and polymer light-emitting diodes (OLEDs and PLEDs, respectively) have received much attention for their potential applications as light sources and in flat-panel displays, due to their potential for fabrication over large areas, lightweights, rapid responses, low power consumption, and wide viewing angles.[1–4] Flexible OLEDs have been considered as next-generation devices for applied science and technology ever since their invention in 1992.[5] Nevertheless, their efficiency conversions, full color displays, and lifetimes remain major problems that must be solved if they are to find wide applicability. Typically, vacuum evaporation is used to deposit small molecules onto the substrates in such devices, but this approach is expensive and has environmental concerns. In contrast, polymer materials can be deposited onto their substrates through spin-coating, inkjet printing, or roll-to-roll fabrication from solution, providing the attractive features of uniform distribution over large areas and low cost. OLEDs are fabricated with one or more semiconducting organic layers—including a hole-injection/transporting layer (HITL), an electron-emitting layer (EML), and an electron-injection/transporting layer (EITL)—sandwiched between the two electrodes. For the purpose of increasing the efficiency of high-performance OLEDs, charge injection and transport from both the anode and cathode must be balanced, with their recombination occurring in the electron-emitting layer.[6,7] The HITL is an interfacial layer positioned between the indium tin oxide (ITO) anode and the EML; it can improve charge injection and charge transport from the ITO anode to the EML. HITL materials should have the following properties: an energy level for its highest occupied molecular orbital (HOMO) located between those of the ITO anode and the EML material; minimized absorption of visible light emitted from the EML; a high glass transition temperature (T_g) to elevate the device endurance through minimized degradation by Joule heat generation during device driving.[8–10] Several small-molecule HITL materials have found common use, including 4,4′,4″-tris-[*N*-(naphthalene-2-yl)-*N*-phenyl-amino]triphenylamine (2-TNATA),[11,12] 1,1-Bis[(di-4-tolylamino)phenyl]cyclohexane (TAPC),[13,14] and copper phthalocyanine (CuPc).[15] The triphenylamine functional group has been investigated thoroughly; it is considered a promising HITL material because of its appropriate energy level and good hole injection/transporting ability.[16] The small molecules for OLED devices are regularly incorporated using

[a]*Institute of Applied Chemistry, National Chiao Tung University, HsinChu, 300 Taiwan. E-mail: cyzhu@mail.nctu.edu.tw*
[b]*Department of Materials and Optoelectronic Science, Center for Nanoscience and Nanotechnology, National Sun Yat-Sen University, Kaohsiung, 804, Taiwan. E-mail: kuosw@faculty.nsysu.edu.tw*

†Electronic supplementary information (ESI) available: Experimental details of DSC, UV and PL data through thermal curing of TPABZ behaviour. See DOI: 10.1039/c5py00882d

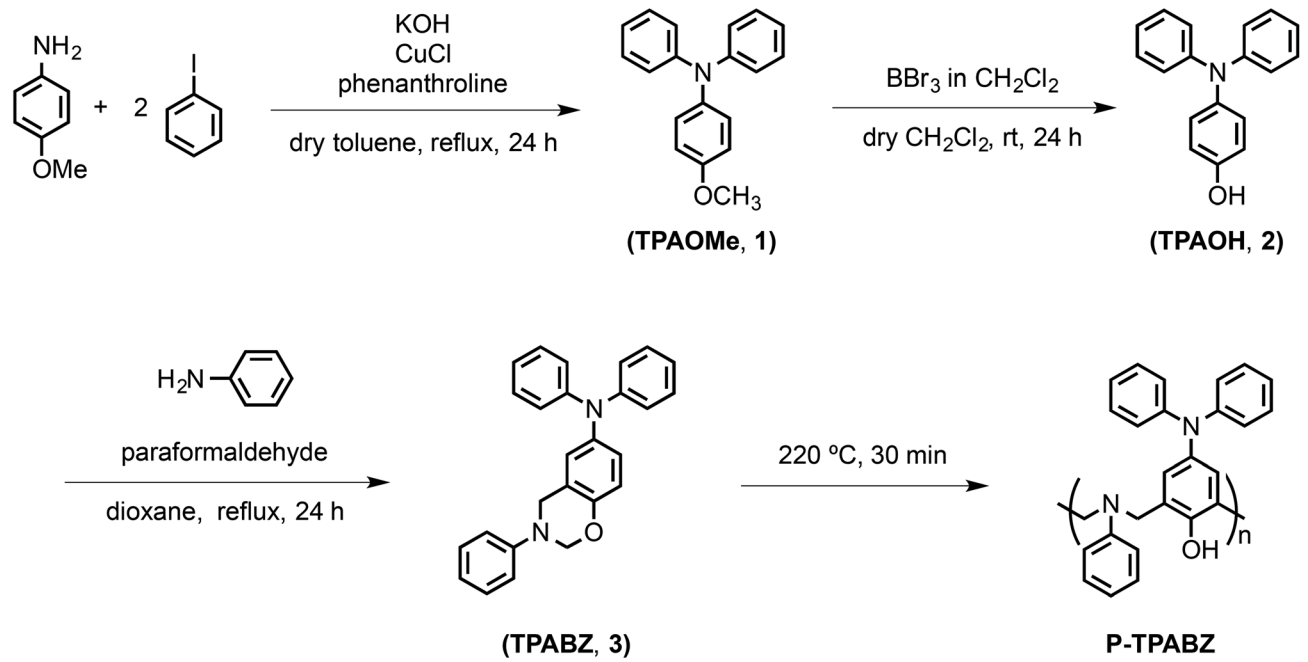

Scheme 1 Synthesis of TPABZ and the structure of P-TPABZ.

high-vacuum vapor deposition, which allows the fabrication of well-defined multilayers with relatively simple structures. Small organic compounds can also be purified, through crystallization or sublimation, to a high degree prior to deposition. Nevertheless, small molecules are prone to morphological damage in OLEDs, through, for example, recrystallization and/or diffusion into another layer, especially at elevated operating temperatures.[17,18] In addition, the need for vacuum processes in the preparation of OLEDs can be expensive and time-consuming when using large-area substrates.[19]

Relative to small molecules, polymers and oligomers can display greater morphological stability and resistance to molecular diffusion between the layers of an OLED. Polymers must be assembled in such devices through solution processing: a rapid and inexpensive process that can be extended to large-area substrates. Nevertheless, using solution processes to create multilayer structures in OLEDs can be challenging, with the possibility of deposition of a layer from solution leading to partial dissolution of the preceding layer. Therefore, hole injection/transporting materials assembled through solution processing have mainly been based on poly(3,4-ethylenedioxythiophene)/polystyrenesulfonate (PEDOT:PSS), which can be deposited from aqueous solutions and is insoluble in the organic solvents used for subsequent deposition of HITL/EML polymers during OLED fabrication.[20,21] In addition, PEDOT:PSS has high conductivity (*ca.* 1–10 S m^{-1}), a suitable ionization potential (Ip: *ca.* −5.2 eV), and good hole injection ability.[22–24] There is, however, a clear drawback: PEDOT:PSS is a strongly acidic polymer that can degrade an OLED and limit its lifetime.[25] Therefore, efforts to develop new HITL materials exhibiting excellent resistance to organic solvents, but featuring neither the hydrophilic nor ionic functionality, have been actively pursued.

Benzoxazine chemistry dates back to the 1940s, when Burke *et al.* described the first syntheses; the polymerization ability of benzoxazine structures was fully investigated in the 1970s.[26–28] Benzoxazine monomers are heterocyclic compounds featuring an oxazine ring; they are synthesized through a Mannich reaction from a phenol, formaldehyde, and a primary amine, with wide structural flexibility in their molecular design.[29–32] The polymerization process and the resulting polymer have several outstanding characteristics: no requirement for a catalyst, no generation of byproducts, low water absorption, flame retardance, a stable dielectric constant, low surface free energy, and near-zero shrinkage during the curing reaction.[33–39] In this study, we synthesized TPABZ, a new triphenylamine derivative (Scheme 1) incorporating a benzoxazine functional group, in three steps and then investigated its applicability as an HITL material in OLEDs. We tested the thermal properties of TPABZ, which is readily polymerized, through ring-opening polymerization of its benzoxazine unit, upon heating at 220 °C for 30 min. We also investigated the physical and electrical properties of cured TPABZ (P-TPABZ), which appears to be a suitable hole injection/transport material for OLEDs because its appropriate HOMO energy level (−5.16 eV) and high-energy lowest unoccupied molecular orbital (LUMO, −1.68 eV) form a stepwise energy ladder with great potential for electron blocking. Furthermore, we fabricated multilayer OLEDs through successive spin-coating of the HITL materials (ITO/TPABZ or P-TPABZ/NPB/Alq_3/LiF/Al); the performance of the device incorporating P-TPABZ was excellent (EQE_{max} = 2.44%; LE_{max} = 8.42 cd A^{-1}; PE_{max}: 4.34 lm W^{-1}).

Experimental section

Materials and characterization

All reagents were obtained from Aldrich or Acros and used as received. All solvents were purchased from Tedia (USA) and distilled over CaH_2 prior to use. ^1H and ^{13}C nuclear magnetic resonance (NMR) spectra were recorded using an Inova 500 Instrument; DMSO-d_6 was the standard solvent; chemical shifts are reported in parts per million (ppm). Fourier transform infrared (FTIR) spectroscopy was performed using a Bruker Tensor 27 apparatus and the conventional KBr disk method; each spectrum was recorded from 32 scans at a spectral resolution of 4 cm^{-1}. A TA Q-20 differential scanning calorimeter, operated under a N_2 atmosphere flow rate of 50 mL min^{-1}, was used to determine dynamic curing kinetics; a sample (*ca.* 5 mg) was placed in a sealed aluminum sample pan. Glass transition temperatures and dynamic curing scans were recorded at a heating rate of 20 °C min^{-1} over the temperature range from 25 to 330 °C. A TA Q-50 thermogravimetric analyzer, operated under a N_2 atmosphere flow rate of 60 mL min^{-1}, was used to measure the thermal stability; a sample (*ca.* 6 mg) was placed in a Pt cell and heated at a rate of 20 °C min^{-1} from 35 to 800 °C. An HP 8453 Diode-Array Spectrophotometer and a Hitachi F4500 Luminescence Spectrometer were used to record UV–Vis spectra and PL spectra, respectively. A BAS 100 B/W Electrochemical Analyzer, operated at a scan rate of 100 mV s^{-1}, was used for cyclic voltammetry (CV); the potentials were measured using Ag/Ag^+ (0.01 M $AgNO_3$) as the reference electrode and ferrocene/ferrocenium (Fc/Fc^+) as the internal standard. Atomic force microscopy (AFM) was performed in dynamic force mode using a Hitachi High-Tech Instrument Scanning Probe Microscope (AFM5300E) to examine the surface morphology and estimate the thickness and root-mean-square (rms) roughness of deposited films.

Synthesis of 4-methoxy-*N*,*N*-diphenylaniline (TPAOMe, 1)

A mixture of 4-methoxyaniline (2.00 g, 16.2 mmol), iodobenzene (8.30 g, 40.7 mmol), potassium hydroxide (7.30 g, 126 mmol), copper(I) chloride (0.330 g, 3.30 mmol), and 1,10-phenanthroline (0.580 g, 3.20 mmol) in dry toluene (15 mL) in a 50 mL two-neck flask was heated under reflux for 24 h under a N_2 gas flow. After evaporating the solvent under reduced pressure, the residue was purified through column chromatography (SiO_2; *n*-hexane/EtOAc, 8 : 1) to yield a white powder (66%). ^1H NMR (DMSO-d_6, ppm): 3.74 (s, ArOCH_3, 3H), 6.91–6.95 (m, NCC*H*, 6H), 6.95–6.96 (d, NCCHCHC*H*, 2H), 7.01–7.03 (d, OCC*H*, 2H), 7.23–7.26 (t, NCCHC*H*, 4H). ^{13}C NMR (DMSO-d_6, ppm): 55.53 (ArO*C*H3, 1C), 115.06, 129.30, 139.87, 156.03 (NAr*C*OCH3, 6C), 121.86, 122.22, 127.934, 147.64 (NAr*C*, 12C). IR (KBr, cm^{-1}): 1035, 1242 (Ar–O–CH3 stretching); 1492, 1506, 1587 (aromatic C–C stretching); 2835, 2951, 3035 (aromatic C–H stretching).

Synthesis of 4-hydroxy-*N*,*N*-diphenylaniline (TPAOH, 2)

A solution of boron tribromide (2.05 g, 8.2 mmol) in dry CH_2Cl_2 (8 mL) was added *via* a syringe to a solution of **1** (1.5 g, 5.5 mmol) in dry CH_2Cl_2 (27 mL) in a 50 mL two-neck flask, cooled in an ice-bath under a N_2 gas flow. The solution was then left to stand at room temperature for 24 h. The solution was filtered through silicon dioxide after adding activated charcoal, and the filtrate was washed with 1 M NaOH (aq.) and then dried ($MgSO_4$). Evaporation of the solvent yielded a white product (62%). ^1H NMR (DMSO-d_6, ppm): 6.75–6.77 (d, OCC*H*, 2H), 6.90–6.91 (m, NCC*H*, 6H), 6.92–6.93 (N–CCHCHC*H*, 2H), 7.21–7.24 (t, NCCHC*H*, 4H), 9.40 (s, ArO*H*, 1H). ^{13}C NMR (DMSO-d_6, ppm): 116.38, 129.20, 138.19, 154.51 (NAr*C*OH), 121.51, 121.84, 127.95, 147.77 (NAr*C*). IR (KBr, cm^{-1}): 1492, 1506, 1587 (aromatic C–C stretching); 2835, 2951, 3035 (aromatic C–H stretching); 3361, 3388, 3415, 3535 (ArOH).

Synthesis of *N*,*N*, 3-triphenyl-3,4-dihydro-2*H*-benzo[*e*][1,3]-oxazin-6-amine (TPABZ, 3)

Aniline (1.07 g, 11.5 mmol) was added *via* a syringe under N_2 to a solution of **2** (1.5 g, 5.7 mmol) and paraformaldehyde (0.69 g, 23 mmol) in dry dioxane (25 mL) in a 50 mL two-neck flask, cooled in an ice bath. The solution was heated under reflux for 24 h and then the solvent was evaporated under reduced pressure. CH_2Cl_2 was added; the solution was washed with 1 M NaOH (aq.) and then dried ($MgSO_4$). The product was purified through column chromatography (SiO_2; *n*-hexane/EtOAc, 3 : 1), yielding a yellow powder (55%). ^1H NMR (DMSO-d_6, ppm): 4.60 (s, CCH_2N, 2H), 5.44 (s, NCH_2O, 2H), 6.72–6.74 (d, OCC*H*, 1H), 6.81–6.97 (m, NCC*H* and NCCCC*H*, 9H), 7.11–7.13 (d, NCCCC*H*, 2H), 7.22–7.26 (t, NCCC*H*, 6H). ^{13}C NMR (DMSO-d_6, ppm): 48.97 (CCH_2N, 1C), 78.85 (NCH_2O, 1C), 117.13, 117.41, 120.38, 121.97, 122.2, 122.48, 124.46, 125.46, 129.13, 129.33, 139.76, 147.59, 147.72, 150.66 (Ar*C*, 24C). IR (KBr, cm^{-1}): 943 (oxazine ring out-of-plane CH bending); 1226 (Ar–O–C stretching); 1491, 1599, 1587 (aromatic C–C stretching); 2835, 2951, 3035 (aromatic C–H stretching).

Fabrication of OLEDs

ITO glass (sheet resistance: 25 Ω per square) was cleaned with UV-ozone. The electroluminescent device configuration was ITO/TPABZ or P-TPABZ/NPB/Alq_3/LiF/Al. The HITL material (TPABZ or P-TPABZ) was deposited through spin-coating at 4000 rpm and 20 s (deposited thickness: 15 nm) onto ITO glass; the other materials were deposited sequentially through vacuum deposition at 10^{-6} torr. Thermal treatment to give P-TPABZ was performed at 220 °C for 30 min under a N_2 atmosphere. A deposition rate of NPB was 1.0 Å s^{-1}; the thickness of deposited NPB in the OLED was 15 nm. LiF was thermally deposited at a deposition rate at 0.1 Å s^{-1} (deposited thickness of LiF: 1 nm). The cathode was capped with the Al metal at an evaporation rate of 4.0 Å s^{-1} (deposited thickness of Al: 100 nm). A Keithley 2400 SourceMeter and a Newport 1835C Optical Meter, equipped with an 818ST Silicon Photodiode, were used to measure the current density and brightness, respectively, of the OLEDs with respect to voltage. A Hitachi F4500 Luminescence Spectrometer was used to record electroluminescence (EL) spectra. The efficiencies of devices incorporating the different types of HITLs were measured at

least three times; the standard deviation of each measured efficiency was less than 8%.

Results and discussion

Synthesis and characterization of the new cross-linkable triphenylamine derivative TPAB

Scheme 1 presents the three-step synthesis of TPABZ and the structure of cured-TPABZ (P-TPABZ). We formed the triphenylamine unit through nucleophilic substitution of iodobenzene by 4-methoxyaniline, giving TPAOMe. Hydrolysis with boron tribromide gave TPAOH, the OH group of which took part in a Mannich reaction with paraformaldehyde and aniline to give the target compound (TPABZ). ^{1}H NMR, ^{13}C NMR, and FTIR spectra confirmed the chemical structures of TPAOMe, TPAOH, and TPABZ. Fig. 1 displays the ^{1}H NMR spectra of TPAOMe, TPAOH, and TPABZ in DMSO-d_6. The signals of TPAOMe [Fig. 1(a)] at 3.74 and 6.91–7.26 ppm represent the protons of the methoxyl group and the aromatic rings, respectively. Hydrolysis caused the signal for the methoxyl group of TPAOMe to disappear and a signal to appear at 9.40 ppm for the proton of the OH group of TPAOH [Fig. 1(b)], along with the signals for the aromatic protons at 7.01–7.03 ppm (O–CC*H*) moving slightly upfield to 6.75–6.77 ppm. Characteristic signals of TPABZ [Fig. 1(c)] appeared at 4.60 and 5.44 ppm (integration ratio, 1 : 1), corresponding to the protons of the benzoxazine ring (CCH_2N and NCH_2O); the aromatic protons appeared at 6.72–7.26 ppm. In addition, the signal of the OH group of TPAOH disappeared, confirming the success of the Mannich reaction.

Fig. 2 presents the ^{13}C NMR spectra of TPAOMe, TPAOH, and TPABZ in DMSO-d_6. The spectrum of TPAOMe featured a signal at 55.53 ppm for the carbon nucleus of the methoxyl group; this signal disappeared after hydrolysis. The spectrum of TPABZ featured signals at 48.97 and 78.85 ppm, corresponding to the carbon nuclei of the benzoxazine ring (C*C*H_2N and N*C*H_2O), as well as signals for all the aromatic carbon nuclei in the range of 117.13–150.66 ppm. Fig. 3 displays the FTIR spectra of TPAOMe, TPAOH, and TPABZ, recorded using the conventional KBr disk method. The characteristic absorption bands of TPAOMe [Fig. 3(a)] appeared at 1035 and 1242 cm^{-1} for the symmetrical and asymmetrical stretching of the aryl alkyl ether; at 1492, 1506, and 1587 cm^{-1} for aromatic C–C stretching; and at 2835, 2951, and 3035 cm^{-1} for aromatic C–H stretching. After hydrolysis [Fig. 3(b)], the characteristic absorption bands of the aryl alkyl ether had disappeared, with an absorption band appearing for the phenolic group of TPAOH near 3500 cm^{-1}. The characteristic absorption bands of TPABZ [Fig. 3(c)] appeared at 943 cm^{-1} for oxazine ring out-of-plane CH bending and at 1226 cm^{-1} for oxazine ring ether stretching. Taken together, the ^{1}H NMR, ^{13}C NMR, and FTIR spectroscopic data confirmed the chemical structure of TPABZ and its successful synthesis.

Thermal properties of TPABZ and P-TPABZ

We used DSC and FTIR to investigate the polymerization behavior of TPABZ. Fig. 4 presents DSC thermograms of the pure TPABZ monomer, recorded after each heating stage. The DSC curve of the uncured TPABZ featured a sharp melting point with endothermic energy (57.48 J g^{-1}) at 126.5 °C, suggesting

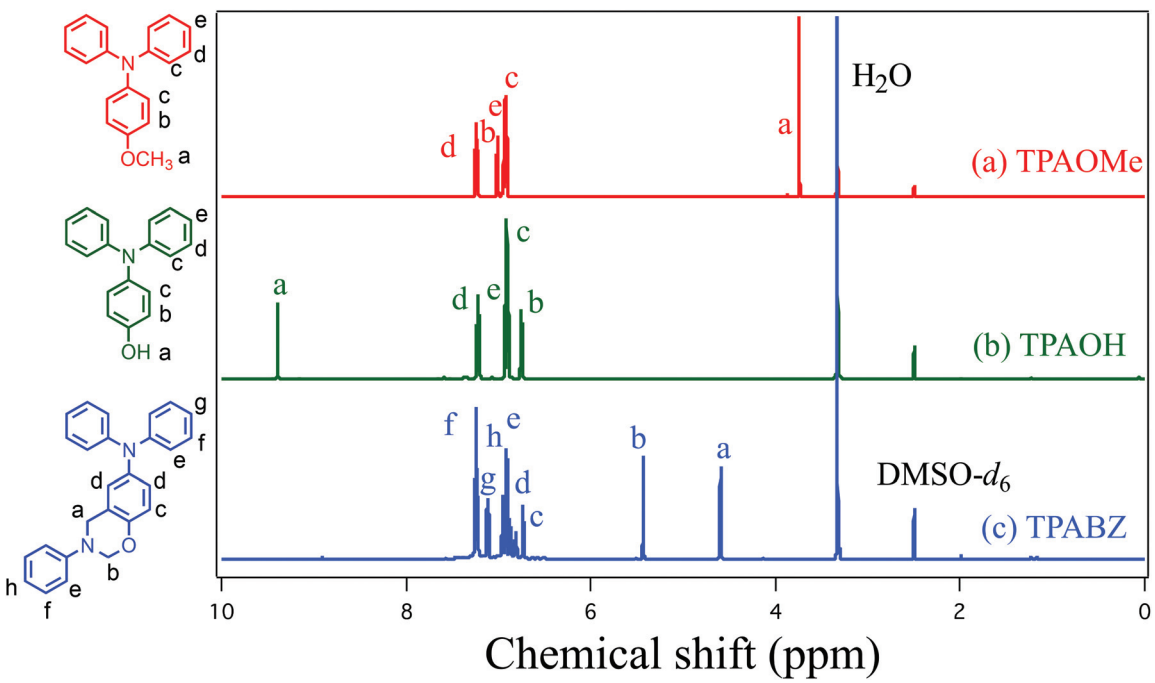

Fig. 1 ^{1}H NMR spectra of TPAOMe, TPAOH, and TPABZ in DMSO-d_6.

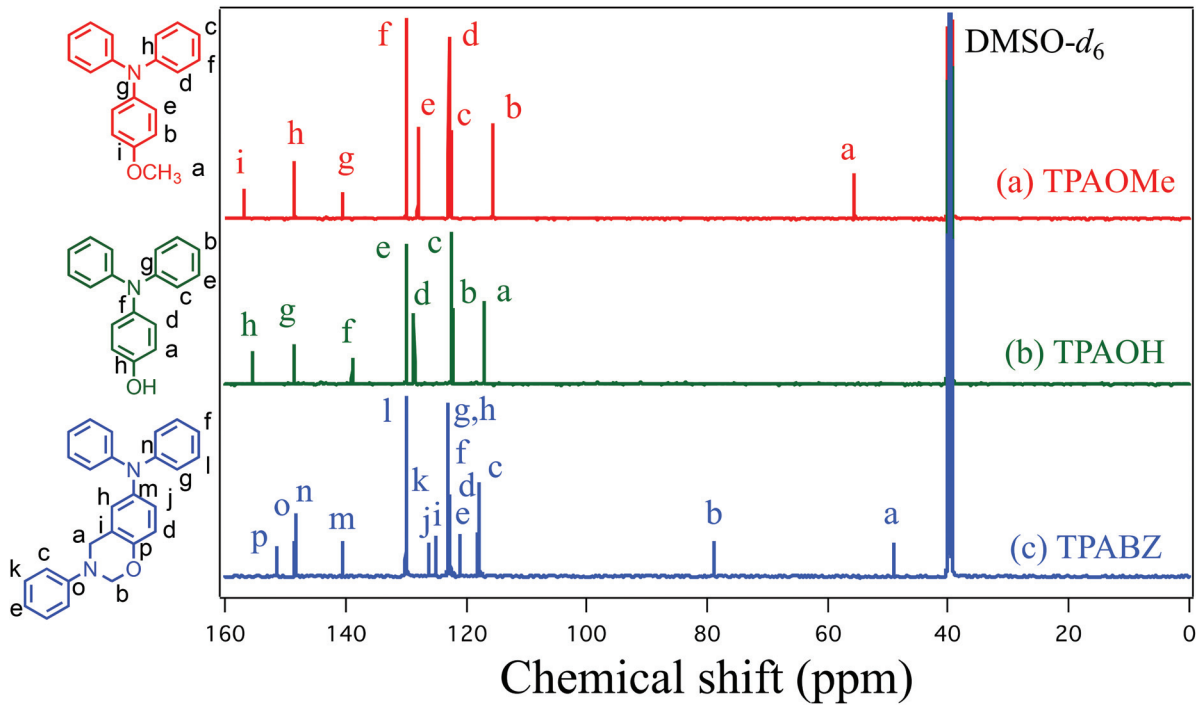

Fig. 2 ^{13}C NMR spectra of TPAOMe, TPAOH, and TPABZ in DMSO-d_6.

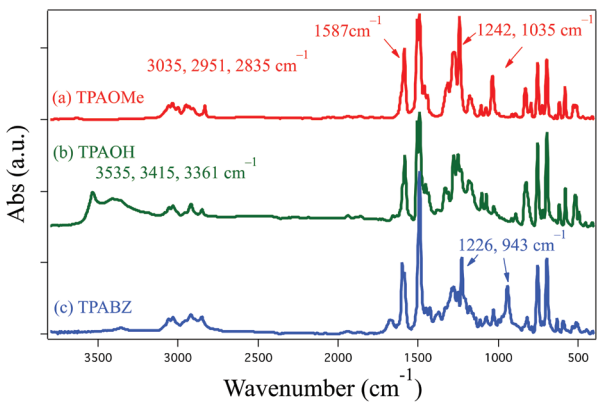

Fig. 3 FTIR spectra of TPAOMe, TPAOH, and TPABZ.

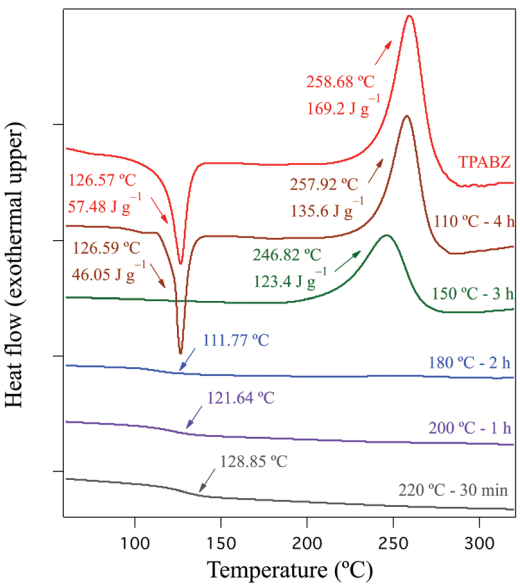

Fig. 4 DSC thermograms of TPABZ, recorded after each heating stage.

the high purity of TPABZ, and an exothermic peak with a maximum at 258.6 °C and a reaction heat of 169.2 J g^{-1}. The DSC thermogram curve of cured TPABZ, after thermal curing at 110 °C for 4 h, was similar to that of the uncured TPABZ. After thermal curing at 150 °C for 3 h, however, the melting peak disappeared and the exothermic peak of the polymerization reaction decreased, with a maximum at 246.8 °C and a heat of 123.4 J g^{-1}. The exothermic peak of the polymerization reaction nearly disappeared completely after thermal curing at 180 °C for 2 h (Fig. S1†). The glass transition temperature (T_g) was higher after curing at higher thermal curing temperatures; for P-TPABZ, the value of T_g was 128.8 °C (Fig. S2†). Thus, our sample of TPABZ was of high purity and its polymerization occurred through a simple thermal curing process without a catalyst; in addition, P-TPABZ exhibited great thermal stability. To understand the thermal curing process of polymerization that occurred during DSC, we used FTIR spectroscopy to characterize the structures formed from TPABZ at various temperatures (Fig. 5). The intensities of the characteristic absorption bands of TPABZ at 943 (oxazine ring out-of-plane

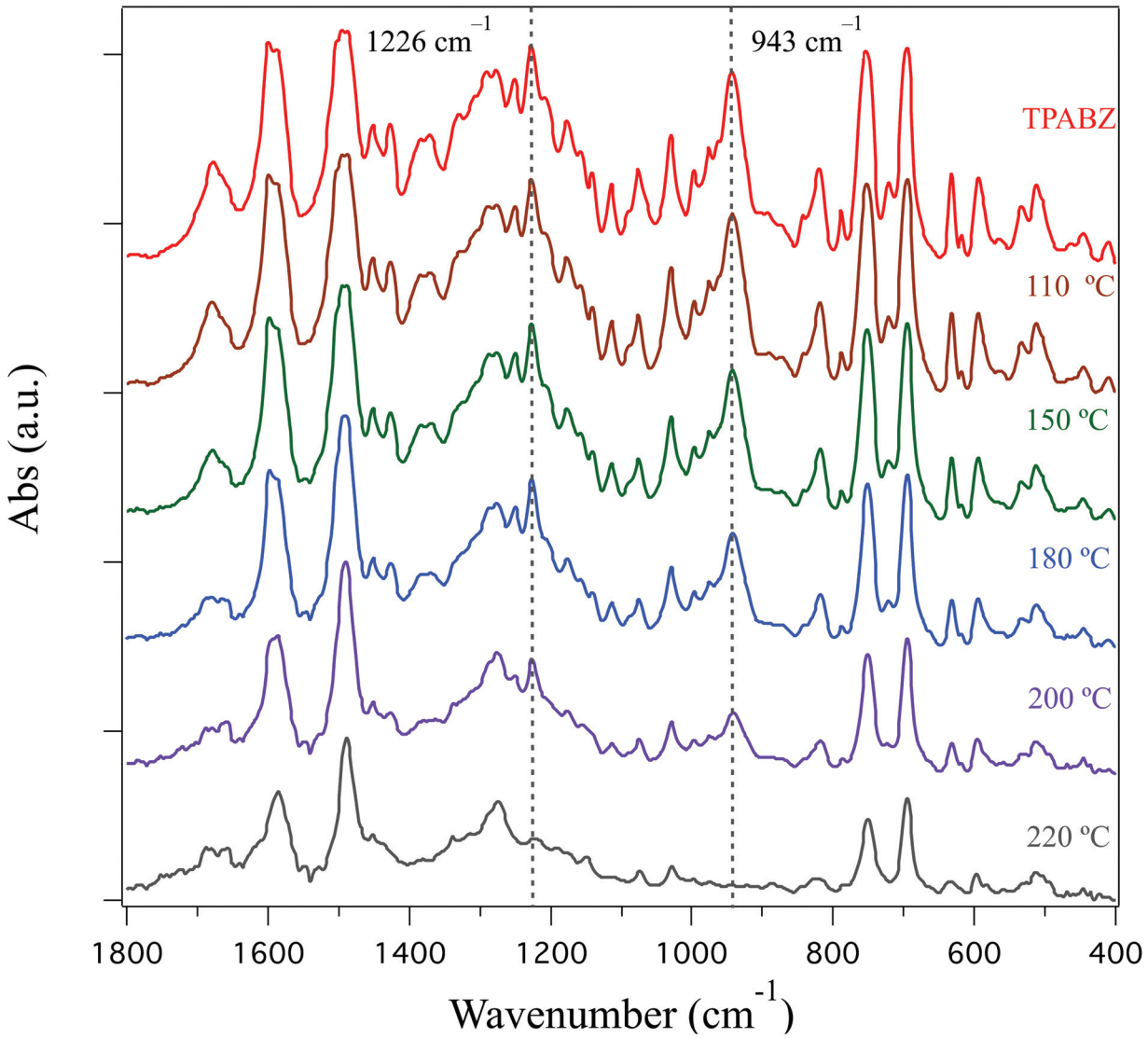

Fig. 5 FTIR spectra of TPABZ, recorded at various temperatures.

CH bending) and 1226 (Ar–O–C stretching) cm^{-1} decreased after thermal curing at 150 °C. These two characteristic absorption bands of TPABZ did not disappear completely after thermal curing at 180 and 200 °C, suggesting incomplete ring-opening polymerization of the oxazine after thermal curing at these temperatures. In contrast, these two characteristic absorption bands disappeared completely after thermal curing at 220 °C, implying a complete ring-opening polymerization of the oxazine after thermal curing at this temperature. Thus, the FTIR spectroscopic data of TPABZ recorded at various temperatures were consistent with the data obtained using DSC.[40,41] Fig. 6 displays the results of TGA of TPABZ and P-TPABZ, performed under a N_2 atmosphere with heating at a rate of 20 °C min^{-1} from 35 to 800 °C. The thermal stability, characterized as the decomposition temperature required for 5 wt% loss (T_d), of TPABZ was 218 °C, with a char yield of 24.7%. P-TPABZ exhibited excellent thermal stability, with a value of T_d of 350 °C and a char yield of 45.5%. Therefore, both DSC and TGA confirmed that P-TPABZ had great thermal stability (values of T_g and T_d are 128.8 and 350 °C, respectively; Table 1).

Physical and electrical properties of TPABZ and P-TPABZ

We used UV–Vis spectroscopy and CV to examine the physical and electrical properties of TPABZ and P-TPABZ as a means of testing the suitability for use as HITL materials in OLEDs. Fig. 7 displays the UV–Vis spectra of films of TPABZ and P-TPABZ. Both compounds provided a single absorption band at 306 nm, which we attribute to the energy level of their triphenylamine functional groups.[16,42,43] The band gap energies (E_g) of the films of TPABZ and P-TPABZ, obtained from their onset absorption wavelengths in the UV–Vis absorption spectra, were 3.49 and 3.48 eV, respectively ($E_g = 1240/\lambda$). Fabrication of multilayered OLEDs and PLEDs through solution-

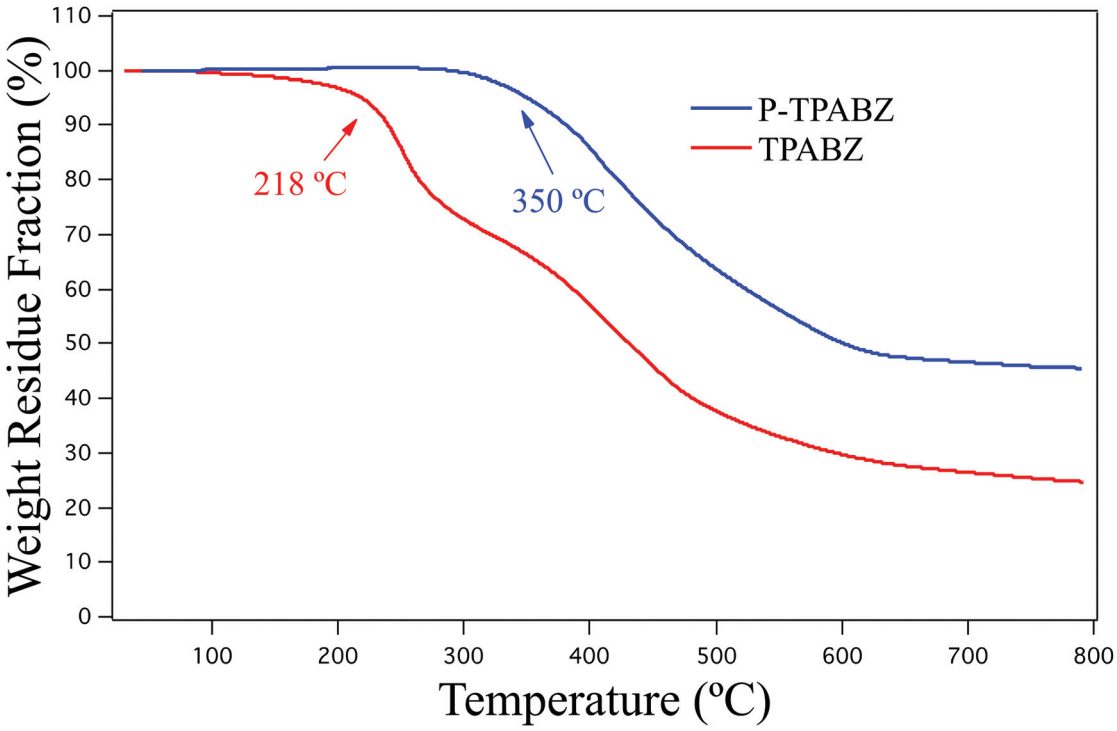

Fig. 6 TGA traces of TPABZ and P-TPABZ.

Table 1 Thermal and electrical properties of TPABZ and P-TPABZ

	T_d (°)	T_g (°C)	E_g [a] (eV)	$E_{ox,onset}$ [b] (eV)	HOMO[c] (eV)	LUMO[d] (eV)
TPABZ	218		3.49	0.37	−5.17	−1.68
P-TPABZ	350	128.85	3.48	0.36	−5.16	−1.68

[a] E_g was obtained from the onset absorption wavelength (λ_{onset}) from the UV-Vis absorption spectrum in the film state: $E_g = 1240/\lambda$. [b] $E_{ox,onset}$ values were measured by CV. [c] HOMO = −(4.8 + $E_{ox,onset}$) eV. [d] LUMO = E_g + HOMO.

processing requires a film to be insoluble in the solvent used for the subsequent deposition process. Therefore, we investigated the solvent-resistance (Fig. S3†) of TPABZ and P-TPABZ films by measuring the UV–Vis absorption spectra after rinsing with chlorobenzene (a typical solvent for solution-processing). The solvent-resistance of P-TPABZ was greater than that of TPABZ, due to its polymeric structure.

We applied an electrochemical analyzer, operated at a scan rate of 100 mV s^{-1} and using Ag/Ag^+ (0.01 M $AgNO_3$) as the reference electrode and ferrocene/ferrocenium (Fc/Fc^+) as the internal standard, to record the potentials of TPABZ and P-TPABZ in the thin film state (spin-coated from 1,1,2,2-tetrachloroethane onto ITO glass). The HOMO energy level can be estimated from the onset oxidation potential ($E_{ox,\ onset}$), the ionization potential revealed in the cyclic voltammogram, using the equation HOMO = −($E_{ox,\ onset}$ + 4.8) eV. Fig. 8(a) presents the cyclic voltammogram of TPABZ, from which we estimated the HOMO energy level to be −5.17 eV (onset oxidation potential: 0.37 V). From Fig. 8(b) we estimated the HOMO energy level of P-TPABZ to be −5.16 eV (onset oxidation potential: 0.36 V). Furthermore, we estimated the LUMO energy levels of TPABZ and P-TPABZ both to be −1.68 eV (Table 1), calculated from their HOMO energy levels and band gap energies (E_g). Thus, the electrochemical characteristics of P-TPABZ were nearly identical to those of TPABZ, suggesting that both compounds have appropriate HOMO energy levels and high LUMO energy levels with electron blocking ability. According to their excellent physical and electrical properties, we suspected that P-TPABZ and TPABZ would be potentially useful HITL materials for fabricating OLEDs.

A homogeneous film of each layer of materials is necessary when fabricating a multilayered OLED or PLED to ensure high efficiency and long lifetime, especially when operated at high temperatures.[44,45] Thus, we used AFM (dynamic force mode) to investigate the morphologies of films of TPABZ and P-TPABZ, spin-coated from 1,1,2,2-tetrachloroethane onto ITO glass. The morphological images of TPABZ and P-TPABZ in Fig. 9 reveal that both films had uniform surface morphologies. TPABZ exhibited great film-forming properties and a homogeneous surface morphology, with a root-mean-square (rms) roughness of 0.81 nm. Furthermore, P-TPABZ (after thermal curing at 220 °C for 30 min) also exhibited a homogeneous surface morphology (rms roughness: 0.78 nm), consistent with the thermal curing reactions of benzoxazines occurring with near-zero shrinkage.[36,38]

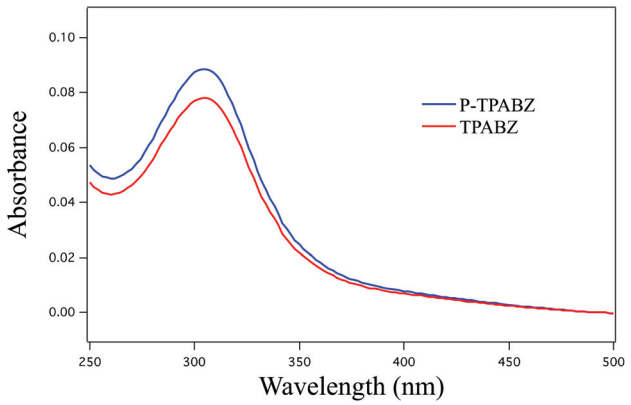

Fig. 7 UV–Vis spectra of films of TPABZ and P-TPABZ.

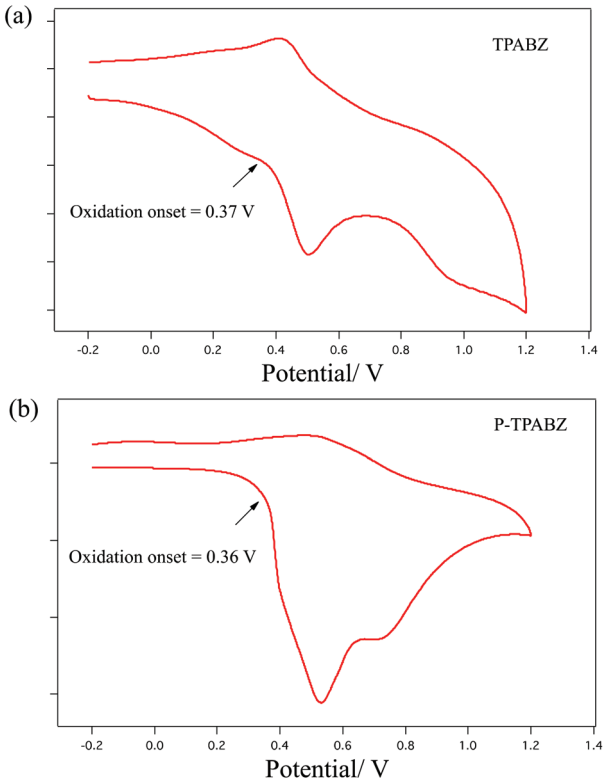

Fig. 8 Cyclic voltammograms of films of (a) TPABZ and (b) P-TPABZ.

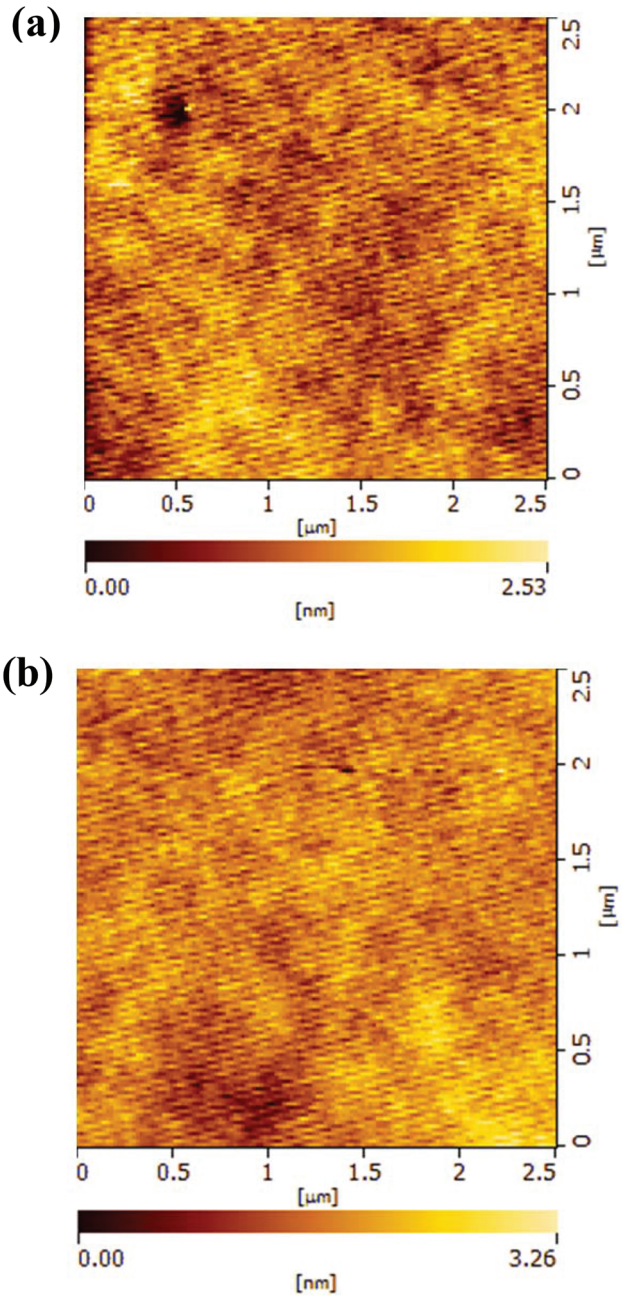

Fig. 9 AFM images of the surface morphologies of films of (a) TPABZ (rms = 0.81 nm) and (b) P-TPABZ (rms = 0.78 nm) on ITO glass.

Fluorescence OLED incorporating TPABZ or P-TPABZ as HITL materials (ITO/TPABZ or P-TPABZ/NPB/Alq_3/LiF/Al)

We fabricated hole-only devices [ITO/HITL (50 nm)/Al] to investigate the hole injection/transporting properties of TPABZ and P-TPABZ. Here, we spin-coated the HITL materials using tetrachloroethane as the solvent. The current density of the hole-only device incorporating P-TPABZ was higher than that of the device based on TPABZ (Fig. 10), suggesting greater hole injecting/transporting ability of the former device. Notably, however, the HOMO energy levels for TPABZ and P-TPABZ were nearly identical. Therefore, the hole injection/transporting properties improved as a result of the polymeric structure and the higher intermolecular hole drifting mobility of P-TPABZ; that is, the chemically cross-linked structure elevated the hole injection/transporting ability. Thus, devices featuring the polymeric structure of P-TPABZ would display greater hole injection and transporting ability when compared with those of the corresponding devices incorporating the small molecule TPABZ.

To further determine the suitability of using P-TPABZ as an HITL material, we processed TPABZ and P-TPABZ for Alq_3 (normal green light-emitting) fluorescent OLEDs. Scheme 2

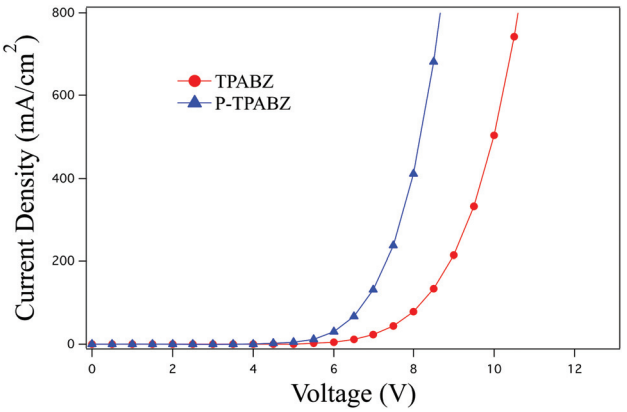

Fig. 10 Current density–voltage of hole-only devices incorporating TPABZ and P-TPABZ.

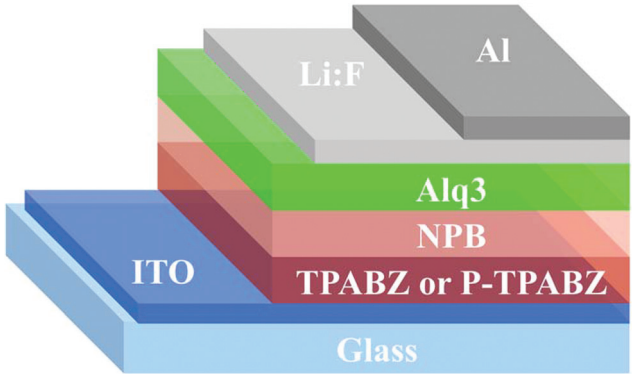

Scheme 2 Schematic representation of the structure of the fluorescent OLEDs: ITO/TPABZ or P-TPABZ/NPB/Alq_3/LiF/Al.

presents the structures of these OLEDs, featuring sequential layers of TPABZ or P-TPABZ (HITL; 15 nm), NPB (hole transporting layer; 15 nm), Alq_3 (emitting layer as well as electron transporting layer; 60 nm), LiF (electron injecting layer; 1 nm), and Al (electrode; 100 nm) on ITO (transparent anode). We deposited the films of TPABZ and P-TPABZ through spin-coating (4000 rpm, 20 s) onto ITO glass, and the other materials through sequential vacuum-deposition at 10^{-6} torr. The EL spectra of the fluorescent OLEDs (Fig. S4†) featured one emission peak at 513 nm, indicating that the EL originated from the film of Alq_3 and that TPABZ or P-TPABZ functioned only as the hole injection/transporting material.

Fig. 11 displays the current density–voltage–luminance (*I*–*V*–*L*) performance of these green fluorescent OLEDs incorporating TPABZ and P-TPABZ as HITL materials; Table 2 lists the EL characteristics. The current density of the fluorescent OLED based on P-TPABZ was higher than that of the device incorporating TPABZ at the same voltage [Fig. 11(a)], consistent with the results for the hole-only devices (*i.e.*, P-TPABZ exhibited better hole injection/transporting properties). The turn-on voltage (luminescence at 1 cd m^{-2}) of the device incorporating P-TPABZ was 3.40 V, lower than that of the OLED based on TPABZ (4.27 V). Fig. 11(b) displays the *L*–*I* characteristics of these devices. The maximum luminescence of the device featuring P-TPABZ as the HITL material (32 347 cd m^{-2}) was 1.8 times higher than that of the device incorporating TPABZ (18 051 cd m^{-2}). Fig. 11(c)–(e) present the external quantum efficiency (EQE), luminance efficiency (LE), and power efficiency (PE), respectively, of these OLEDs plotted with respect to the current density. The EQE, LE, and PE of the

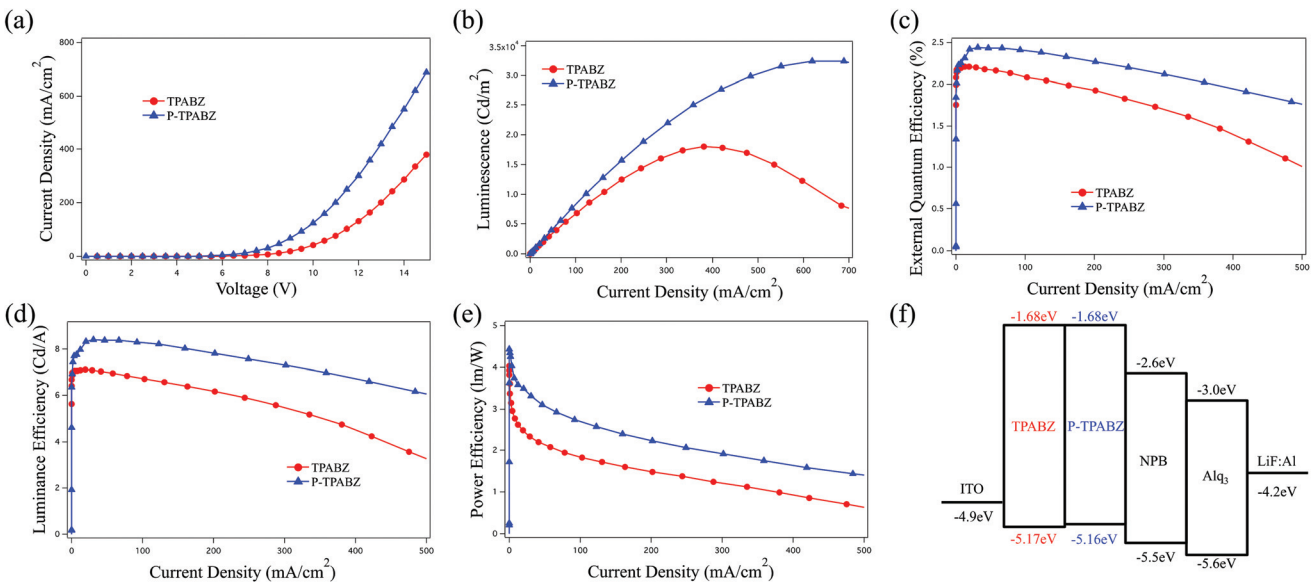

Fig. 11 Characteristics of devices having the structure ITO/TPABZ or P-TPABZ/NPB/Alq_3/LiF/Al: (a) current density–voltage; (b) luminance–current density; (c) EQE–current density; (d) LE–current density; (e) PE–current density; and (f) energy level.

Table 2 Characteristics of electroluminescent OLEDs having the structure ITO/TPABZ or P-TPABZ/NPB/Alq_3/LiF/Al

	V_{on} (V)	EQE (%)	LE_{max} (cd A^{-1})	PE_{max} (lm W^{-1})	B_{max} (cd m^{-2})
TPABZ	4.27	2.21	7.10	4.03	18 051
P-TPABZ	3.20	2.44	8.42	4.34	32 347

device featuring P-TPABZ as the HITL material (2.44%, 8.32 cd A^{-1}, and 4.34 lm W^{-1}, respectively) were superior to those of the device incorporating TPABZ (2.21%, 7.10 cd A^{-1}, and 4.03 lm W^{-1}, respectively). As mentioned above, the hole injection and transporting abilities of P-TPABZ were better than those of TPABZ. Therefore, the improvement in the efficiency performance of the fluorescent device incorporating P-TPABZ as the HITL material could also be attributed to its polymeric structure and higher intermolecular hole drifting mobility, because the electrode, all of the other layer materials, and the thickness of each layer were identical in each OLED. It is particularly noteworthy that the efficiency performance (EQE: 2.44%; LE: 8.32 cd A^{-1}; PE: 4.34 lm W^{-1}) of the device having the structure ITO/P-TPABZ/NPB/Alq_3/LiF/Al was superior to that of the corresponding device based on PEDOT:PSS, the commercial hole injecting material (EQE: 2.1%; LE: 7.16 cd A^{-1}) in Fig. S6.† Thus, the EQE performance was even 1.17 times higher than that of the device based on commercial PEDOT:PSS.[46]

Conclusions

We have synthesized a new thermally cross-linkable triphenylamine derivative containing a benzoxazine functional group (TPABZ). Its product after thermal curing, P-TPABZ, is a suitable hole injection/transport material for use in OLEDs, due to its appropriate HOMO energy level (−5.16 eV), for forming a stepwise energy ladder, and its high LUMO energy level (−1.68 eV), with great ability for electron blocking. From investigations of hole-only devices incorporating TPABZ and P-TPABZ, we found that the hole injection/transporting ability was greater for the latter compound, due to its polymeric structure (chemical cross-linking) and higher intermolecular hole drifting mobility. Furthermore, from analyses of multilayered OLEDs (ITO/TPABZ or P-TPABZ/NPB/Alq_3/LiF/Al), we observed good performance when using P-TPABZ as the HITL (EQE: 2.44%; LE_{max}: 8.42 cd A^{-1}; PE_{max}: 4.34 lm W^{-1}).

Acknowledgements

This study was supported financially by the Ministry of Science and Technology, Taiwan (contracts MOST103-2221-E-110-079-MY3 and MOST102-2221-E-110-008-MY3). We thank Professor Chien-Hong Cheng (National Tsing Hua University) for assistance and support during the construction and characterization of the OLEDs, and Professor Feng-Chih Chang for contributing to the writing of this paper.

References

1 S. R. Forrest, *Nature*, 2004, **428**, 911–918.
2 A. Misra, P. Kumar, M. N. Kamalasanan and S. Chandra, *Semicond. Sci. Technol.*, 2006, **21**, R35–R47.
3 M. A. McCarthy, B. Liu, E. P. Donoghue, I. Kravchenko, D. Y. Kim, F. So and A. G. Rinzler, *Science*, 2011, **332**, 570–573.
4 J. W. Park, D. C. Shin and S. H. Park, *Semicond. Sci. Technol.*, 2011, **26**, 034002.
5 G. Gustafsson, Y. Cao, G. M. Treacy, F. Klavetter, N. colaneri and A. J. Heeger, *Nature*, 1992, **357**, 477–479.
6 J. H. Burroughes, D. D. C. Bradley, A. R. Brown, R. N. Marks, K. Mackay, R. H. Friend, P. L. Burns and A. B. Holmes, *Nature*, 1990, **347**, 539–541.
7 M. Strukelj, F. Papadimitrakopoulos, T. M. Miller and L. J. Rothberg, *Science*, 1995, **267**, 1969–1972.
8 H. Aziz and Z. D. Popovic, *Chem. Mater.*, 2004, **16**, 4522–4532.
9 S. K. Kim, J. H. Lee and J. W. Park, *J. Nanosci. Nanotechnol.*, 2008, **8**, 5247–5251.
10 Y. Park, B. Kim, C. Lee, A. Hyun, S. Jang, J. H. Lee, Y. S. Gal, T. H. Kim, K. S. Kim and J. Park, *J. Phys. Chem. C*, 2011, **105**, 4843–4850.
11 Y. Shirota, Y. Kuwabara, H. Inada, T. Wakimoto, H. Nakada, Y. Yonemoto, S. Kawami and K. Imai, *Appl. Phys. Lett.*, 1994, **65**, 807–809.
12 D. Heithecker, A. Kammoun, T. Dobbertin, T. Riedl, E. Becker, D. Metzdorf, D. Schneider, H.-H. Johannes and W. Kowalsky, *Appl. Phys. Lett.*, 2003, **82**, 4178–4180.
13 P. M. Borsenberger, L. Pautmeier, R. Richert and H. Bässler, *J. Chem. Phys.*, 1991, **94**, 8276–8281.
14 P. M. Borsenberger, E. H. Magin and J. J. Fitzgerald, *J. Phys. Chem.*, 1993, **97**, 8250–8253.
15 S. A. Van Slyke1, C. H. Chen1 and C. W. Tang, *Appl. Phys. Lett.*, 1996, **69**, 2160–2162.
16 P. Cias, C. Slugovc and G. Gescheidt, *J. Phys. Chem. A*, 2011, **115**, 14519–14525.
17 S. Tokito, H. Tanaka, K. Noda, A. Okada and Y. Taga, *Appl. Phys. Lett.*, 1997, **70**, 1929–1931.
18 W. C. Lin, W. B. Wang, Y. C. Lin, B. Y. Yu, Y. Y. Chen, M. F. Hsu, J. H. Jou and J. J. Shyue, *Org. Electron.*, 2009, **10**, 581–586.
19 F. So, J. Kido and P. Burrows, *MRS Bull.*, 2008, **33**, 663–669.
20 S. A. Carter, M. Angelopoulos, S. Karg, P. J. Brock and J. C. Scott, *Appl. Phys. Lett.*, 1997, **70**, 2067–2069.
21 W. H. Kim, A. J. Makinen, N. Nikolov, R. Shashidhar, H. Kim and Z. H. Kafafi, *Appl. Phys. Lett.*, 2002, **80**, 3844–3846.
22 G. Heywang and F. Jonas, *Adv. Mater.*, 1992, **4**, 116–118.
23 L. Groenendaal, F. Jonas, D. Freitag, H. Pielartzik and J. R. Reynolds, *Adv. Mater.*, 2000, **12**, 481–494.

24 Q. Xu, J. Ouyang, Y. Yang, T. Ito and J. Kido, *Appl. Phys. Lett.*, 2003, **83**, 4695–4697.
25 M. P. de Jong, L. J. van Ijzendoorn and M. J. A. de Voigt, *Appl. Phys. Lett.*, 2000, **77**, 2255–2257.
26 W. J. Burke, *J. Am. Chem. Soc.*, 1949, **71**, 609–612.
27 H. Schreiber, *German Patent*, 2 255 504, 1973.
28 G. Riess, J. M. Schwob and G. Guth, *Abstr. Pap. Am. Chem. Soc.*, 1984, **188**, 85.
29 B. Kiskan, B. Koz and Y. Yagci, *J. Polym. Sci., Part A: Polym. Chem.*, 2009, **47**, 6955–6961.
30 R. Kudoh, A. Sudo and T. Endo, *Macromolecules*, 2010, **43**, 1185–1187.
31 H. Xu, Z. Lu and G. Zhang, *RSC Adv.*, 2012, **2**, 2768–2772.
32 M. Imran, B. Kiskan and Y. Yagci, *Tetrahedron Lett.*, 2013, **54**, 4966–4969.
33 N. N. Ghosh, B. Kiskan and Y. Yagci, *Prog. Polym. Sci.*, 2007, **32**, 1344–1391.
34 C. F. Wang, Y. C. Su, S. W. Kuo, C. F. Huang, Y. C. Sheen and F. C. Chang, *Angew. Chem., Int. Ed.*, 2006, **45**, 2248–2251.
35 Y. Yagci, B. Kiskan and N. N. Ghosh, *J. Polym. Sci., Part A: Polym. Chem.*, 2009, **47**, 5565–5576.
36 M. R. Vengatesan, S. Devaraju, K. Dinakaran and M. Alagar, *J. Mater. Chem.*, 2012, **22**, 7559–7566.
37 C. F. Wang, S. F. Chiou, F. H. Ko, J. K. Chen, C. T. Chou, C. F. Huang, S. W. Kuo and F. C. Chang, *Langmuir*, 2007, **23**, 5868–5871.
38 C. F. Wang, F. C. Chang and S. W. Kuo, *Hand book of polybenzoxazine Resins*, 2011, vol. 33, p. 579.
39 M. G. Mohamed, K. C. Hsu and S. W. Kuo, *Polym. Chem.*, 2015, **6**, 2423–2433.
40 W. H. Hu, K. W. Huang and S. W. Kuo, *Polym. Chem.*, 2012, **3**, 1546–1554.
41 M. G. Mohamed, C. H. Hsiao, K. C. Hsu, F. H. Lu, H. K. Shih and S. W. Kuo, *RSC Adv.*, 2015, **5**, 12763–12772.
42 L.-Z. Borg, A. L. Domanski, A. Breivogel, M. Bürger, R. Berger, K. Heinze and R. Zentel, *J. Mater. Chem. C*, 2013, **1**, 1223–1230.
43 Y. Tao, C. Yang and J. Qin, *Chem. Soc. Rev.*, 2011, **40**, 2943–2970.
44 D. F. O'Brien, P. E. Burrows, S. R. Forrest, B. E. Koene, D. E. Loy and M. E. Thompson, *Adv. Mater.*, 1998, **10**, 1108–1112.
45 P. N. M. dos Anjos, H. Aziz, N.-X. Hu and Z. D. Popovic, *Org. Electron.*, 2002, **3**, 9–13.
46 Y. L. Chu, C. C. Cheng, Y. C. Yen and F. C. Chang, *Adv. Mater.*, 2012, **24**, 1894–1898.